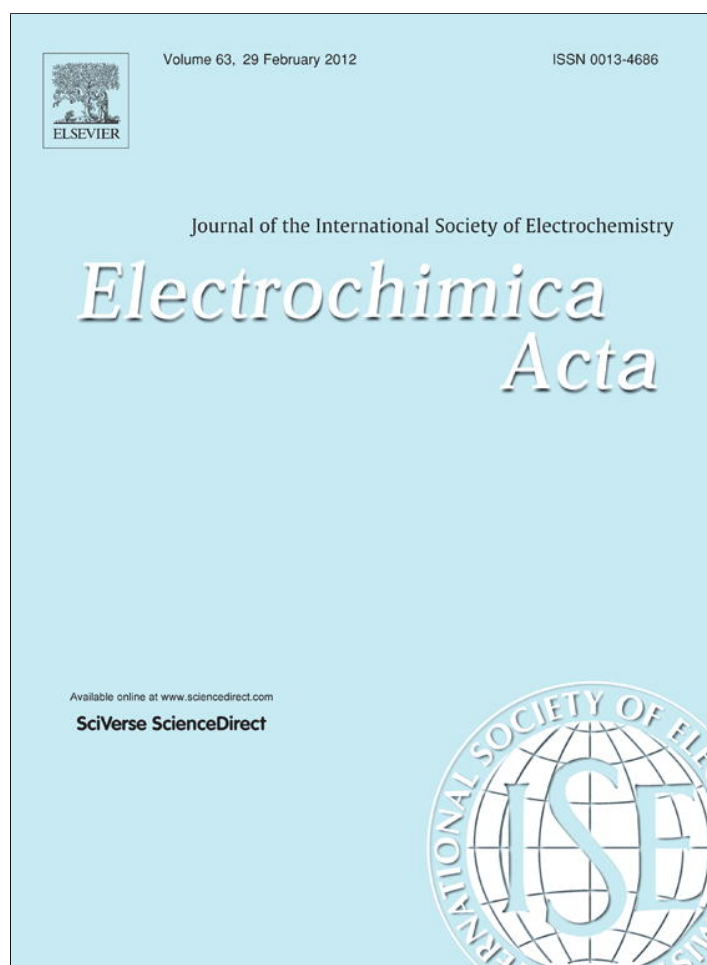


Provided for non-commercial research and education use.  
Not for reproduction, distribution or commercial use.



This article appeared in a journal published by Elsevier. The attached copy is furnished to the author for internal non-commercial research and education use, including for instruction at the authors institution and sharing with colleagues.

Other uses, including reproduction and distribution, or selling or licensing copies, or posting to personal, institutional or third party websites are prohibited.

In most cases authors are permitted to post their version of the article (e.g. in Word or Tex form) to their personal website or institutional repository. Authors requiring further information regarding Elsevier's archiving and manuscript policies are encouraged to visit:

<http://www.elsevier.com/copyright>



# Microwave-assisted hydrothermal synthesis of nanostructured spinel $\text{Li}_4\text{Ti}_5\text{O}_{12}$ as anode materials for lithium ion batteries

Jian Liu<sup>a</sup>, Xifei Li<sup>a</sup>, Jinli Yang<sup>a</sup>, Dongsheng Geng<sup>a</sup>, Yongliang Li<sup>a</sup>, Dongniu Wang<sup>a</sup>, Ruying Li<sup>a</sup>, Xueliang Sun<sup>a,\*</sup>, Mei Cai<sup>b</sup>, Mark W. Verbrugge<sup>b</sup>

<sup>a</sup> Department of Mechanical and Materials Engineering, University of Western Ontario, London, ON, Canada N6A 5B9

<sup>b</sup> General Motors R&D Center, Warren, MI 48090-9055, USA

## ARTICLE INFO

### Article history:

Received 19 October 2011

Received in revised form

12 December 2011

Accepted 13 December 2011

Available online 26 December 2011

### Keywords:

$\text{Li}_4\text{Ti}_5\text{O}_{12}$

Microwave-assisted hydrothermal method

Lithium ion batteries

Anode material

## ABSTRACT

Nanoflower-like and nanoparticle spinel  $\text{Li}_4\text{Ti}_5\text{O}_{12}$  were synthesized by a microwave-assisted hydrothermal (MH) method following calcination. As-prepared  $\text{Li}_4\text{Ti}_5\text{O}_{12}$  was characterized by scanning electron microscopy, transmission electron microscopy, X-ray powder diffraction and cyclic voltammetry. The nanoflower-like and nanoparticle  $\text{Li}_4\text{Ti}_5\text{O}_{12}$  exhibited discharge capacities of 176.7 and 109.8  $\text{mAh g}^{-1}$ , respectively, for the first cycle, and maintained reversible capacities of 138.4 and 91.7  $\text{mAh g}^{-1}$ , respectively, at a 1.1 C-rate (200  $\text{mA g}^{-1}$ ) after 100 cycles. The better performance of nanoflower-like  $\text{Li}_4\text{Ti}_5\text{O}_{12}$  relative to nanoparticle  $\text{Li}_4\text{Ti}_5\text{O}_{12}$  is attributed to the larger specific surface area and shorter  $\text{Li}^+$  diffusion path of the former relative to the latter. The MH preparation process is straightforward and fast; thus it shows promise for widespread lithium ion battery applications.

© 2012 Elsevier Ltd. All rights reserved.

## 1. Introduction

Lithium ion batteries (LIBs) are the most developed energy storage system for portable devices, electric vehicles (EVs) and hybrid electric vehicles (HEVs) due in large part to their high energy density and long cycling life [1–4]. At present, graphite is widely used in commercial LIBs as the anode material, but it suffers from poor abuse tolerance for EV and HEV applications [5]. Recently, spinel  $\text{Li}_4\text{Ti}_5\text{O}_{12}$  has attracted much interest as a promising anode (negative electrode) material for LIBs due to its unique advantages [4–20]. The potential for unusually high-power cells has spurred much of this research [21–24]. The working voltage of spinel  $\text{Li}_4\text{Ti}_5\text{O}_{12}$  is approximately at 1.55 V (vs.  $\text{Li}/\text{Li}^+$ ), which avoids the formation of a conventional solid electrolyte interphase (e.g. as seen over graphite), as the electrolyte is not exposed to strongly reducing potentials; thus, high coulombic efficiencies result [18]. Moreover, the zero-strain of spinel  $\text{Li}_4\text{Ti}_5\text{O}_{12}$  upon lithiation and delithiation yields excellent structural stability and reversibility during charge and discharge processes [19]. In addition, the high lithium ion mobility in  $\text{Li}_4\text{Ti}_5\text{O}_{12}$  provides good rate capability in LIBs, which is desirable for traction applications [20].

In recent years, much effort has been devoted to developing nanoscaled spinel  $\text{Li}_4\text{Ti}_5\text{O}_{12}$ , which can improve the

charge/discharge rate by shorting diffusion path of electrons and lithium ions. Spinel  $\text{Li}_4\text{Ti}_5\text{O}_{12}$  nanomaterials with different morphologies, such as nanotubes and nanowires [25,26], nanosheets [27,28] and porous microspheres [29], have been successfully synthesized by solvothermal [25] and hydrothermal [26–29] methods. Recently, microwave-assisted hydrothermal (MH) methods have been employed and found to be efficient for the synthesis of nanomaterials [30–37]. MH methods rely on the interactions of dielectric materials, be the liquid or solid, with microwave radiation that causes direct dielectric heating [30]; the process yields very rapid heating relative to less direct conventional hydrothermal (CH) methods [31]. In general, it takes only 1–3 min to heat water up to 100–150 °C by MH methods, while 60–100 min are often required using CH methods [31]. In addition, MH methods have several advantages over CH methods: (1) short reaction time and low-temperature processing [32,33], (2) extremely rapid kinetics of crystallization [34], and (3) low energy consumption [32–34]. Up to now, MH methods have been used successfully to synthesize nanomaterials of  $\text{MnO}_2$  [30],  $\text{WO}_3$  [31],  $\text{Co}_3\text{O}_4$  [35] and  $\text{LiFePO}_4$  [36,37].

Herein, we report the synthesis of nanostructured  $\text{Li}_4\text{Ti}_5\text{O}_{12}$  by a MH method following heat treatment. Nanoflower-like and nanoparticle  $\text{Li}_4\text{Ti}_5\text{O}_{12}$  were obtained at different temperatures. The electrochemical properties of the nanoflower-like and nanoparticle  $\text{Li}_4\text{Ti}_5\text{O}_{12}$  were investigated as anode materials for LIBs. The effect of morphology on the LIB performance of  $\text{Li}_4\text{Ti}_5\text{O}_{12}$  is discussed.

\* Corresponding author. Tel.: +1 519 661 2111x87759; fax: +1 519 661 3020.  
E-mail address: [xsun@eng.uwo.ca](mailto:xsun@eng.uwo.ca) (X. Sun).

## 2. Experimental

### 2.1. Sample preparation and characterization

In a typical process, 191.6 mg LiOH and 1 mL 30% H<sub>2</sub>O<sub>2</sub> were dissolved into 20 mL deionized water, and the mixture was stirred for several minutes until a clear solution was obtained. Then 0.59 mL titanium tetraisopropoxide (TTIP) was dropwise added into the clear solution with stirring. After stirring for 30 min, 15 mL of the obtained solution was transferred to an 80 mL Teflon-lined PTFE autoclave vessel, which was sealed and heated to desired temperatures (130 and 170 °C), with a holding time of 20 min in a microwave-assisted hydrothermal synthesis system (Anton Paar Synthos 3000). After the autoclave was cooled to room temperature, products were collected by centrifugation, washed with deionized water thoroughly, and dried in an oven at 80 °C for 12 h. Last, the as-prepared products were calcined in a quartz tube furnace at 550 °C for 6 h in air.

The materials were characterized by X-ray diffraction (XRD, Rigaku RU-200BVH with a Co-K $\alpha$  source, with  $\lambda = 1.7892 \text{ \AA}$ ), field emission scanning electron microscopy (SEM, Hitachi S4800), transmission electron microscopy (TEM, Hitachi H-7000), and high resolution TEM (HRTEM, JEOL 2010 FEG microscope). N<sub>2</sub> adsorption/desorption isotherms were obtained using a Folio Micromeritics TriStar II Surface Area and Pore Size Analyzer.

### 2.2. Electrochemical characterization

Electrochemical measurements were performed by using coin-type half cells assembled in an argon-filled glove box ([O<sub>2</sub>] < 1 ppm, [H<sub>2</sub>O] < 1 ppm). The electrolyte was 1 M LiPF<sub>6</sub> solution in ethylene carbonate and dimethyl carbonate with a volume ratio of 1:1. To prepare the electrode, the active material powder, acetylene black and polyvinylidene fluoride binder, with a weight ratio of 80:10:10 were mixed until substantially homogeneous, and pasted onto a copper foil. Each electrode foil has a surface area of 1.6 cm<sup>2</sup> and contains active material of ~5 mg. Then the electrode was dried under vacuum at 110 °C for 12 h. The coin cells were cycled at a current density of 200 mA g<sup>-1</sup> with cutoff voltages of 1.0 and 2.5 V by using an Arbin BT-2000 Battery Test System.

## 3. Results and discussion

Fig. 1 shows XRD patterns of the products as-prepared at 130 and 170 °C, and after calcination at 550 °C for 6 h in air. In Fig. 1(a), it can be seen that the product as-prepared at 130 °C is in agreement with lithium titanium oxide hydrate (JCPDS Card No. 47-0123). It

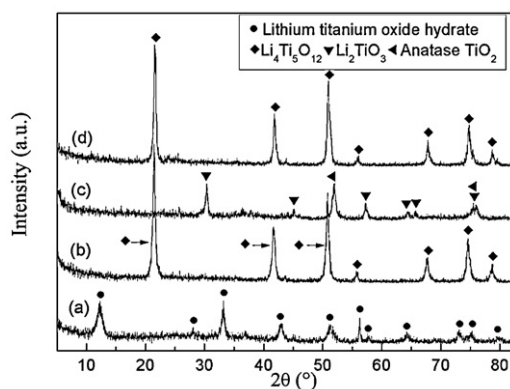


Fig. 1. XRD patterns of the samples synthesized at 130 °C (a, b) and 170 °C (c, d). (a, c) as-prepared, (b, d) after calcination at 550 °C for 6 h in air.

is reported that lithium titanium oxide hydrate can be transformed into spinel Li<sub>4</sub>Ti<sub>5</sub>O<sub>12</sub> by heat treatment above 350 °C [38]. For the sample as-prepared at 170 °C, it is composed of Li<sub>2</sub>TiO<sub>3</sub> (JCPDS Card No. 33-0831) and anatase TiO<sub>2</sub> (JCPDS Card No. 89-4921), as shown in Fig. 1(c). Li<sub>2</sub>TiO<sub>3</sub> and anatase TiO<sub>2</sub> are two precursors widely used for the synthesis of spinel Li<sub>4</sub>Ti<sub>5</sub>O<sub>12</sub> by solid-state methods, as they can react with each other to form spinel Li<sub>4</sub>Ti<sub>5</sub>O<sub>12</sub> at elevated temperatures [39]. After calcined at 550 °C for 6 h, both samples can be indexed as spinel lithium titanate, in accordance with spinel Li<sub>4</sub>Ti<sub>5</sub>O<sub>12</sub> (JCPDS Card No. 49-0207), as seen in Fig. 1(b, d). In the two XRD patterns, no other phases are found, implying high purity of the two samples.

Fig. 2 presents morphologies of Li<sub>4</sub>Ti<sub>5</sub>O<sub>12</sub> synthesized at 130 and 170 °C. In Fig. 2(a), it can be seen that the Li<sub>4</sub>Ti<sub>5</sub>O<sub>12</sub> prepared at 130 °C possesses nanoflower-like spheres with diameters ranging from 500 to 900 nm. Each nanoflower-like sphere comprises many vertical nanosheets. The thickness of the nanosheets is on the order of 10 nm [cf. Fig. 2(b, e)]. Selected area electron diffraction (SAED) pattern [inset in Fig. 2(b)] shows the highly crystalline features of spinel Li<sub>4</sub>Ti<sub>5</sub>O<sub>12</sub>. An HRTEM image of one nanosheet is shown in Fig. 2(e). The lattice distance is measured to be 0.48 nm, which is well in accordance with the  $d_{(111)}$  spacing of spinel Li<sub>4</sub>Ti<sub>5</sub>O<sub>12</sub>. The morphology of the Li<sub>4</sub>Ti<sub>5</sub>O<sub>12</sub> produced at 170 °C is shown in Fig. 2(c, d). This kind of Li<sub>4</sub>Ti<sub>5</sub>O<sub>12</sub> consists of numerous nanoparticles, the size of which varies from tens of nanometers to hundreds of nanometers, as seen in Fig. 2(d). Those nanoparticles agglomerate and form micro-size particles, as shown in Fig. 2(c). Based on the above results, it can be concluded that nanoflower-like and nanoparticle Li<sub>4</sub>Ti<sub>5</sub>O<sub>12</sub> with high purity and high crystallinity are successfully synthesized by the MH method and following heat treatment.

Fig. 3 shows the N<sub>2</sub> adsorption/desorption isotherms and pore size distribution (inset) for the nanoflower-like and nanoparticle Li<sub>4</sub>Ti<sub>5</sub>O<sub>12</sub>. The N<sub>2</sub> adsorption/desorption isotherms of both samples show type IV isotherms (IUPAC classification) with distinct hysteresis loops at high partial pressures, indicating the presence of mesopores and macropores [38]. Nanoflower-like and nanoparticle Li<sub>4</sub>Ti<sub>5</sub>O<sub>12</sub> show similar pore size distributions, with a narrow peak at about 3 nm and a broad peak centered at 19 nm. Brunauer–Emmett–Teller (BET) analysis shows that nanoflower-like Li<sub>4</sub>Ti<sub>5</sub>O<sub>12</sub> has a specific surface area of 46.8 cm<sup>2</sup> g<sup>-1</sup>, which is much larger than that of the similarly measured 12.1 cm<sup>2</sup> g<sup>-1</sup> for the nanoparticle Li<sub>4</sub>Ti<sub>5</sub>O<sub>12</sub>. The pore volumes of nanoflower-like and nanoparticle Li<sub>4</sub>Ti<sub>5</sub>O<sub>12</sub> are 0.21 cm<sup>3</sup> g<sup>-1</sup> and 0.06 cm<sup>3</sup> g<sup>-1</sup>, respectively.

Fig. 4(a, b) shows the cyclic voltammograms (CVs) of nanoflower-like and nanoparticle Li<sub>4</sub>Ti<sub>5</sub>O<sub>12</sub> respectively, for the first three cycles. In the first cycle, one pair of redox peaks appears at 1.48 (reduction) and 1.65 (oxidation) V in nanoflower-like Li<sub>4</sub>Ti<sub>5</sub>O<sub>12</sub>, and 1.44 (reduction) and 1.75 (oxidation) V in nanoparticle Li<sub>4</sub>Ti<sub>5</sub>O<sub>12</sub>. Those two pairs of peaks correspond to the Li<sup>+</sup> insertion (reduction) and extraction (oxidation) processes [27–29]. The potential differences between anodic and cathodic peaks for nanoflower-like Li<sub>4</sub>Ti<sub>5</sub>O<sub>12</sub> and nanoparticle Li<sub>4</sub>Ti<sub>5</sub>O<sub>12</sub> are 0.17 and 0.33 V, respectively, suggesting a lower electrode polarization for the former [40]. Comparing Fig. 4(a) with (b), we can see that the peak currents of anodic and cathodic reactions are comparable for nanoflower-like Li<sub>4</sub>Ti<sub>5</sub>O<sub>12</sub>, while they are asymmetric for nanoparticle Li<sub>4</sub>Ti<sub>5</sub>O<sub>12</sub>. The asymmetric peak currents have been observed in CVs of bulk spinel Li<sub>4</sub>Ti<sub>5</sub>O<sub>12</sub> and can be attributed to the slow lithium ion diffusivity in bulk spinel Li<sub>4</sub>Ti<sub>5</sub>O<sub>12</sub> [26]. It is believed that the agglomeration of nanoparticle Li<sub>4</sub>Ti<sub>5</sub>O<sub>12</sub> after heat treatment is responsible for its asymmetric peak currents in the CVs and less reversible behavior. For nanoflower-like Li<sub>4</sub>Ti<sub>5</sub>O<sub>12</sub>, the thin nanosheets keep their shapes after calcination, and symmetric peak currents in CVs result, along with less polarization. Further

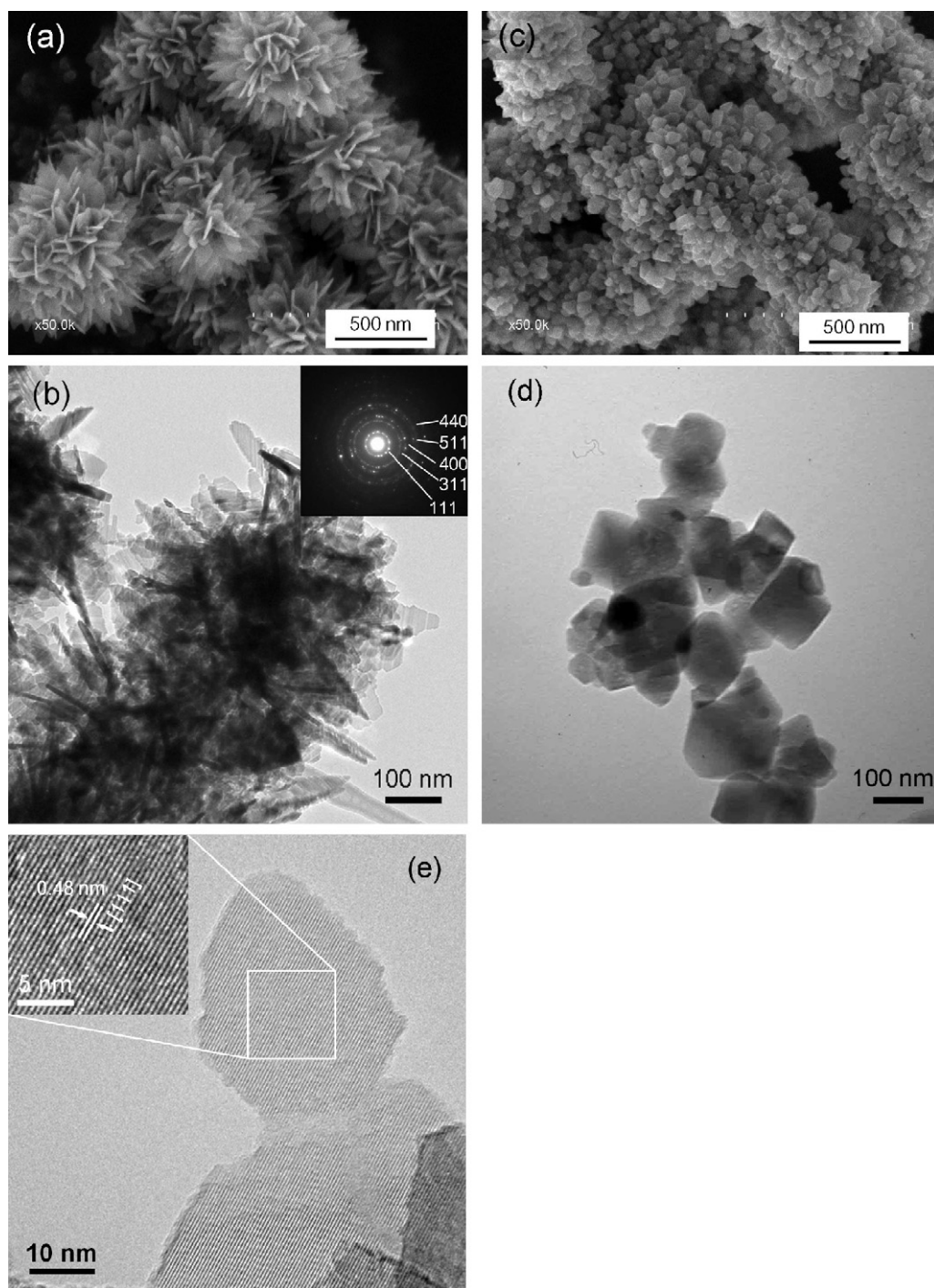


**Fig. 2.** SEM (a, c) and TEM (b, d) images of  $\text{Li}_4\text{Ti}_5\text{O}_{12}$  synthesized at 130 °C (a, b) and 170 °C (c, d). SAED pattern in the inset of (b) shows reflection rings corresponding to spinel  $\text{Li}_4\text{Ti}_5\text{O}_{12}$ . A HRTEM image (e) of  $\text{Li}_4\text{Ti}_5\text{O}_{12}$  synthesized at 130 °C shows the image of lattice fringes and  $d_{(111)} = 0.48$  nm.

supporting this observation, in Fig. 4, it is shown that the initial three cycles almost overlap for nanoflower-like  $\text{Li}_4\text{Ti}_5\text{O}_{12}$ , while slight mismatch is observed for nanoparticle  $\text{Li}_4\text{Ti}_5\text{O}_{12}$ . This difference suggests that nanoflower  $\text{Li}_4\text{Ti}_5\text{O}_{12}$  has better reversibility than nanoparticle  $\text{Li}_4\text{Ti}_5\text{O}_{12}$  during the insertion/extraction processes of  $\text{Li}^+$  into/from  $\text{Li}_4\text{Ti}_5\text{O}_{12}$  [41].

Fig. 5 shows the initial three charge/discharge curves for nanoflower-like and nanoparticle  $\text{Li}_4\text{Ti}_5\text{O}_{12}$  samples. It can be seen that both samples exhibit flat plateaus around 1.5–1.6 V (vs.  $\text{Li}/\text{Li}^+$ ), which correspond to the reversible two phase transition between  $\text{Li}_4\text{Ti}_5\text{O}_{12}$  and  $\text{Li}_7\text{Ti}_5\text{O}_{12}$  [25,26]. For nanoflower-like  $\text{Li}_4\text{Ti}_5\text{O}_{12}$ , the

first discharge capacity reaches as high as  $176.7 \text{ mAh g}^{-1}$ , and an irreversible capacity of 14% is obtained at the first cycle. Nanoparticle  $\text{Li}_4\text{Ti}_5\text{O}_{12}$  delivers a capacity of  $109.8 \text{ mAh g}^{-1}$ , and shows an irreversible capacity of 12% for the first cycle. A similar irreversible capacity during the first charge/discharge cycle has been reported [39,41]. It is usually attributed to the dissolution of surface impurities, such as adsorbed trace water, from the electrodes into the liquid electrolyte [29,31]. From Fig. 5, it can also be seen that nanoflower-like  $\text{Li}_4\text{Ti}_5\text{O}_{12}$  has a smaller difference between charge and discharge plateau potentials than nanoparticle  $\text{Li}_4\text{Ti}_5\text{O}_{12}$ . This result is consistent with the CVs and suggests faster overall

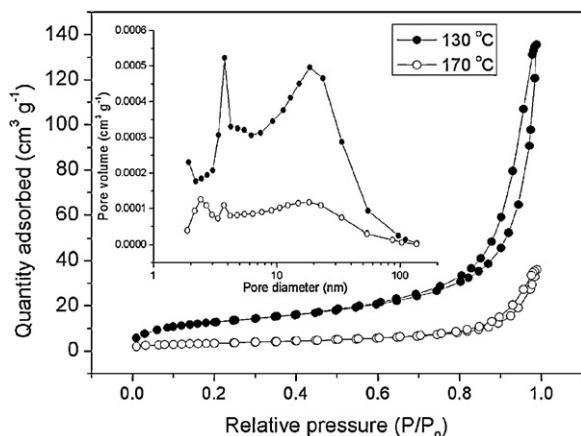


**Fig. 3.**  $N_2$  adsorption–desorption isotherms for  $Li_4Ti_5O_{12}$  synthesized at 130 °C and 170 °C. Inset shows pore size distribution for both samples.

kinetics for the nanoflower-like  $Li_4Ti_5O_{12}$  relative to the nanoparticle  $Li_4Ti_5O_{12}$ . The reason could be attributed to the shorter diffusion path of  $Li^+$  in nanoflower-like  $Li_4Ti_5O_{12}$ . The larger specific surface area of nanoflower-like  $Li_4Ti_5O_{12}$ , relative to the nanoparticle  $Li_4Ti_5O_{12}$  also insures a larger contact area between electrode and electrolyte, which is beneficial for the  $Li^+$  exchange.

The cyclic stabilities of nanoflower-like and nanoparticle  $Li_4Ti_5O_{12}$  were studied at a current density of  $200\text{ mA g}^{-1}$ , and the results are shown in Fig. 6. It can be seen that the specific capacity of nanoparticle  $Li_4Ti_5O_{12}$  remains stable after the first cycle.

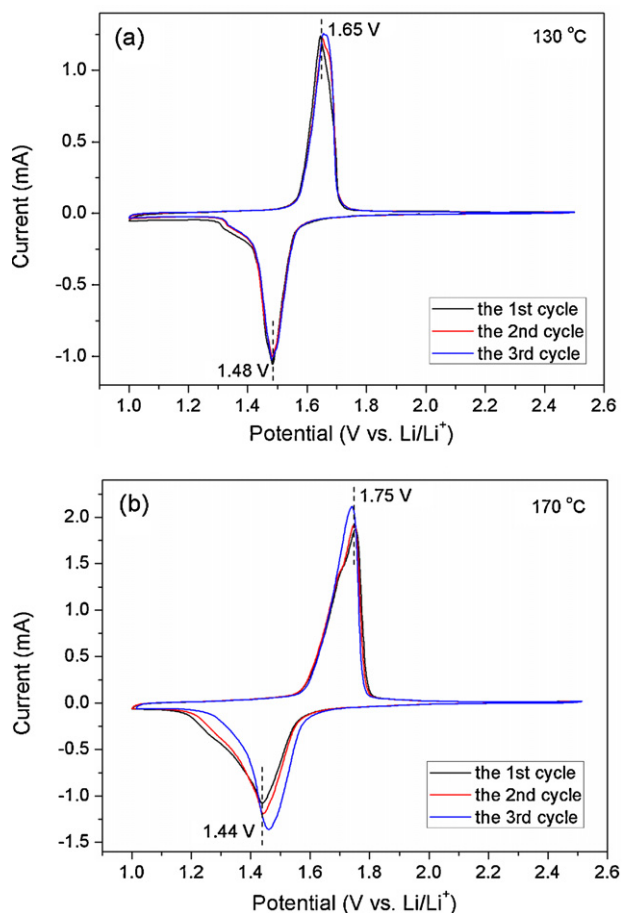


**Fig. 4.** CV curves of  $Li_4Ti_5O_{12}$  prepared at (a) 130 °C and (b) 170 °C in the first three cycles at a scan rate of  $0.2\text{ mV s}^{-1}$ .

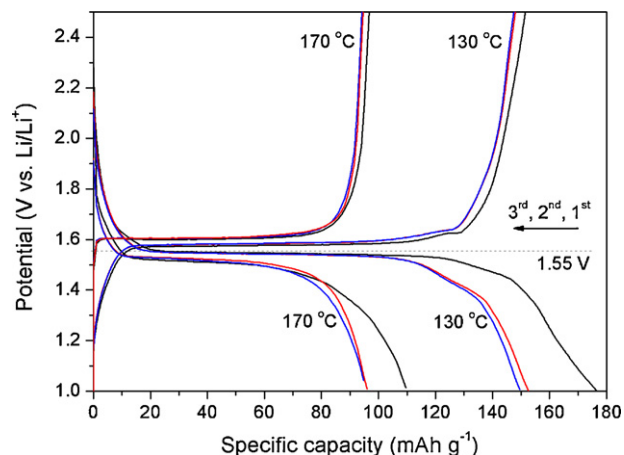


**Fig. 5.** Galvanostatic charge/discharge curves for  $Li_4Ti_5O_{12}$  prepared at 130 °C and 170 °C between 1 and 2.5 V at a current density of  $200\text{ mA g}^{-1}$ .

For nanoflower-like  $Li_4Ti_5O_{12}$ , the irreversible capacity rapidly decreases with upon cycling, and the specific capacity stabilizes after ca. 10 cycles. Both samples exhibit high coulombic efficiencies after the first cycle, effectively 100% for the measurement employed. After 100 cycles, the specific capacities of nanoflower-like and nanoparticle  $Li_4Ti_5O_{12}$  are determined to be  $138.4\text{ mA h g}^{-1}$  and  $91.7\text{ mA h g}^{-1}$ , respectively. It has been widely reported that excellent electrochemical performance could be achieved in high surface area anodes due to short diffusion distance of  $Li^+$  in solid body [25,26,31]. In addition, provided deleterious side reactions are not a concern, smaller particles are beneficial in that they provide increased surface area for electrochemical reaction and reduced overall reaction resistance. Therefore, the larger specific capacity of nanoflower-like  $Li_4Ti_5O_{12}$  than nanoparticle  $Li_4Ti_5O_{12}$  could be attributed to the larger specific surface area and shorter  $Li^+$  diffusion path of the former relative to the latter. In Fig. 6, the capacity retention after 100 cycles is calculated to be 78% and 82% for nanoflower-like and nanoparticle  $Li_4Ti_5O_{12}$ , respectively. It should be noted that the capacity retentions in our case are slightly lower than those reported in some literatures [42,43]. Nonetheless, similar capacity retention of  $Li_4Ti_5O_{12}$  was observed previously [39,41], and the large capacity loss could be attributed to several reasons. One reason is that the annealing temperature of  $Li_4Ti_5O_{12}$  in our case ( $550\text{ °C}$ ) is relatively lower than those ( $700\text{--}800\text{ °C}$ ) in Refs. [42,43]. Higher annealing temperature can lead to better crystallinity of  $Li_4Ti_5O_{12}$  and then a reduced initial capacity loss [44]. However, it can also easily result in the

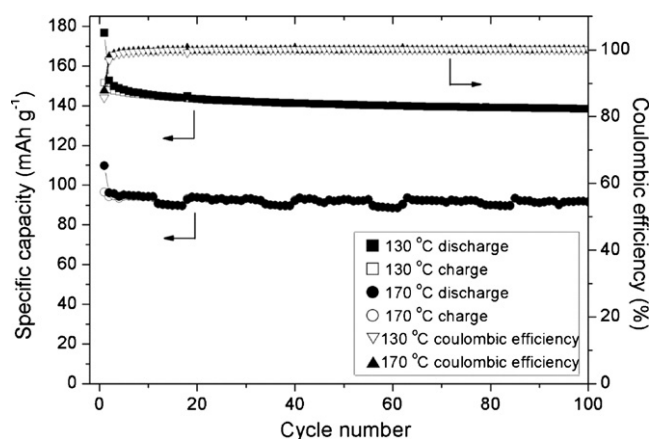


**Fig. 6.** Cycling performance of  $Li_4Ti_5O_{12}$  prepared at 130 °C and 170 °C measured at a current density of  $200\text{ mA g}^{-1}$ .

agglomeration of  $\text{Li}_4\text{Ti}_5\text{O}_{12}$ , which would make its performance worse. Another reason could be the adsorbed trace water, surface defects such as surface vacancies or voids, which are common for nanomaterials but will lead to irreversible capacity [28,29,31]. It should be mentioned that nanoflower-like  $\text{Li}_4\text{Ti}_5\text{O}_{12}$  synthesized by MH method exhibits comparable performance to  $\text{Li}_4\text{Ti}_5\text{O}_{12}$  prepared by CH method, whereas MH process takes much shorter time (20 min) than CH process (12–36 h) [26,28,31].

#### 4. Conclusions

Spinel  $\text{Li}_4\text{Ti}_5\text{O}_{12}$  with nanoflower-like and nanoparticle morphologies were successfully synthesized by a microwave-assisted hydrothermal method and following heat treatment. The nanoflower-like  $\text{Li}_4\text{Ti}_5\text{O}_{12}$  exhibits a layered structure of high specific surface area and provides good reversibility and cycling performance. The nanoflower-like  $\text{Li}_4\text{Ti}_5\text{O}_{12}$  delivered a specific capacity of  $176.7 \text{ mAh g}^{-1}$  during the first cycle, and maintained  $138.4 \text{ mAh g}^{-1}$  after 100 cycles.

#### Acknowledgements

This research was supported by General Motors of Canada, Natural Sciences and Engineering Research Council of Canada (NSERC), Canada Research Chair (CRC) Program, Canada Foundation for Innovation (CFI), Ontario Research Fund (ORF), Ontario Early Researcher Award (ERA) and University of Western Ontario.

#### References

- [1] J.-M. Tarascon, M. Armand, *Nature* 414 (2001) 359.
- [2] K. Kang, Y.S. Meng, J. Br ger, C.P. Grey, G. Ceder, *Science* 311 (2006) 977.
- [3] M. Winter, J.O. Besenhard, M.E. Spahr, P. Nov k, *Adv. Mater.* 10 (1998) 725.
- [4] M. Armand, J.-M. Tarascon, *Nature* 451 (2008) 652.
- [5] N.A. Kaskhedikar, J. Maier, *Adv. Mater.* 21 (2009) 2664.
- [6] K.M. Colbow, J.R. Dahn, R.R. Haering, *J. Power Sources* 26 (1989) 397.
- [7] T. Ohzuku, A. Ueda, *Solid State Ionics* 69 (1994) 201.
- [8] E. Ferg, R.J. Gummow, A. de Kock, M.M. Thackeray, *J. Electrochem. Soc.* 141 (1994) L147.
- [9] T. Ohzuku, A. Ueda, N. Yamamoto, *J. Electrochem. Soc.* 142 (1995) 1431.
- [10] K. Zaghib, M. Armand, M. Gauthier, *J. Electrochem. Soc.* 145 (1998) 3135.
- [11] S. Scharner, W. Weppner, P. Schmid-Baurmann, *J. Electrochem. Soc.* 146 (1999) 857.
- [12] F. Ronci, P. Reale, B. Scrosati, S. Panero, V.R. Albertini, P. Perfetti, M. di Michiel, J.M. Merino, *J. Phys. Chem. B* 106 (2002) 3082.
- [13] A. Gotcher, *Adv. Mater. Process.* 163 (2005) 32.
- [14] I. Plitz, A. Dupasquier, F. Badway, J. Gural, N. Pereira, A. Gmitter, G.G. Amatucci, *Appl. Phys. A: Mater. Sci. Process.* 82 (2006) 615.
- [15] S. Stewart, P. Albertus, V. Srinivasan, I. Plitz, N. Pereira, G. Amatucci, J. Newman, *J. Electrochem. Soc.* 155 (2008) A253.
- [16] P. Liu, E. Sherman, M. Verbrugge, *J. Solid State Electrochem.* 14 (2010) 585.
- [17] J.S. Wang, M.W. Verbrugge, P. Liu, *J. Electrochem. Soc.* 157 (2010) A185.
- [18] J. Shu, *Electrochem. Solid-State Lett.* 11 (2008) A238.
- [19] H. Ge, N. Li, D. Li, C. Dai, D. Wang, *Electrochem. Comm.* 10 (2008) 719.
- [20] S. Takai, M. Kamata, S. Fujine, K. Yoneda, K. Kanda, T. Esaka, *Solid State Ionics* 123 (1999) 165.
- [21] M.W. Verbrugge, P. Liu, *J. Power Sources* 174 (2007) 2.
- [22] M. Imazaki, K. Ariyoshi, T. Ohzuku, *J. Electrochem. Soc.* 156 (2009) A780.
- [23] N. Takami, H. Inagaki, T. Kishi, Y. Harada, Y. Fujita, K. Hoshina, *J. Electrochem. Soc.* 156 (2009) A128.
- [24] K. Zaghib, M. Dontignya, A. Guerfia, P. Charesta, I. Rodriguesa, A. Mauger, C.M. Julien, *J. Power Sources* 196 (2011) 3949.
- [25] D.K. Lee, H.-W. Shim, J.S. An, C.M. Cho, I.-S. Cho, K.S. Hong, D.W. Kim, *Nanoscale Res. Lett.* 5 (2010) 1585.
- [26] J. Li, Z. Tang, Z. Zhang, *Electrochem. Commun.* 7 (2005) 894.
- [27] C. Lai, Y.Y. Dou, X. Li, X.P. Gao, *J. Power Sources* 195 (2010) 3676.
- [28] J. Chen, L. Yang, S. Fang, Y. Tang, *Electrochim. Acta* 55 (2010) 6596.
- [29] L. Shen, C. Yuan, H. Luo, X. Zhang, K. Xu, Y. Xia, *J. Mater. Chem.* 20 (2010) 6998.
- [30] E.K. Nyutu, C.-H. Chen, S. Sithambaram, V.M.B. Crisostomo, S.L. Suib, *J. Phys. Chem. C* 112 (2008) 6786.
- [31] A. Phuruangrat, D.J. Ham, S.J. Hong, S. Thongtem, J.S. Lee, *J. Mater. Chem.* 20 (2010) 1683.
- [32] J. Zhang, Y. Wang, J. Yang, J. Chen, Z. Zhang, *Mater. Lett.* 60 (2006) 3015.
- [33] W. Li, *Mater. Lett.* 62 (2008) 243.
- [34] L. Ma, W. Chen, J. Zhao, Y. Zheng, X. Li, Z. Xu, *Mater. Lett.* 61 (2007) 1711.
- [35] S.Q. Chen, Y. Wang, *J. Mater. Chem.* 20 (2010) 9735.
- [36] A.V. Murugan, T. Muraliganth, A. Manthiram, *J. Phys. Chem. C* 112 (2008) 14665.
- [37] Y. Zhang, H. Feng, X. Wu, L. Wang, A. Zhang, T. Xia, H. Dong, M. Liu, *Electrochim. Acta* 54 (2009) 3206.
- [38] Y. Tang, L. Yang, S. Fang, Z. Qiu, *Electrochim. Acta* 54 (2009) 6244.
- [39] T. Yuan, R. Cai, Z. Shao, *J. Phys. Chem. C* 115 (2011) 4943.
- [40] B. Zhang, H. Du, B. Li, F. Kang, *Electrochem. Solid-State Lett.* 13 (2010) A36.
- [41] Y.F. Tang, L. Yang, Z. Qiu, J.S. Huang, *Electrochem. Commun.* 10 (2008) 1513.
- [42] C. Jiang, E. Hosono, M. Ichihara, I. Honma, H. Zhou, *J. Electrochem. Soc.* 115 (2008) A553.
- [43] A.S. Prakash, P. Manikandan, K. Ramesha, M. Sathiy, J.-M. Tarascon, A.K. Shukla, *Chem. Mater.* 22 (2010) 2857.
- [44] J. Deng, Z. Lu, I. Belharouak, K. Amine, C.Y. Chung, *J. Power Sources* 193 (2009) 816.